DEVELOPMENT AND CHARACTERISATION OF BIOMASS-BASED CELLULOSE HYDROGELS FOR NANOEMULSION DRUG DELIVERY TO THE SKIN

WONG LI CHING

UNIVERSITI SAINS MALAYSIA

2024

DEVELOPMENT AND CHARACTERISATION OF BIOMASS-BASED CELLULOSE HYDROGELS FOR NANOEMULSION DRUG DELIVERY TO THE SKIN

by

WONG LI CHING

Thesis submitted in fulfilment of the requirements for the degree of Doctor of Philosophy

January 2024

ACKNOWLEDGEMENT

The completion of my thesis has been a long and challenging journey, filled with unexpected hurdles that have fueled my personal growth. Along the way, I have been fortunate to meet many amazing people who have supported me in various ways. First and foremost, I must give major props to Dr Goh Choon Fu, my supervisor. He has been a constant source of support, offering invaluable guidance and instilling a profound passion for science that has sustained me through the ups and downs of postgraduate life. I'm also grateful for the invaluable insights and support provided by Assoc Prof Dr Leh Cheu Peng, Prof Vikneswaran a/I Murugaiyah and Dr Yu Kok Hwa in their respective areas of expertise.

I feel extremely grateful and fortunate to have such wonderful friends and science officers who have played a crucial role in teaching me vital skills and imparting valuable advice on using laboratory equipment. Their words of encouragement have truly lifted me during tough times. I would like to express my sincerest gratitude to my fellow labmates, including Salam, Bilal, Soo Chin, Yee Shan, Yi Mo, Hai Long, Estee, Rong Rong and Yoga. I would also like to thank my friends from other labs, including Hema, Boon Keat, Sak Jie, Xin Yi, Siew Mei, Song Thai and Nelson Chear. Additionally, I am deeply grateful for the assistance provided by our science officers, Mr Shahrul, Mr Hilman, Mr Asrul, Mr Hafiz and Mr Asro.

I feel blessed to have received unwavering love from my family for many years. Their constant emotional support serves as a driving force for me to remain motivated and focused on accomplishing my goals.

TABLE OF CONTENTS

ACK	NOWL	EDGEMEN	Ι Τ	ii
ТАВ	LE OF	CONTENT	'S	iii
LIST	OF TA	BLES		ix
LIST	OF FIG	GURES		xi
LIST	OF AE	BREVIAT	IONS	xvii
LIST	OF SY	MBOLS		xviii
ABS	TRAK.			xix
ABS	TRACT	•		xxi
СНА	PTER [*]	1 INTROD	UCTION	1
1.1	Overv	iew		1
1.2	Huma	n skin		2
1.3	Cutan	eous drug	delivery	5
1.4	Hydro	gels		6
	1.4.1	Types of	polymers	7
	1.4.2	Crosslink	ing of hydrogels	8
	1.4.3	Hydrogel	s for cutaneous drug delivery	9
1.5			nass (NWB) cellulose as a source of biopolymer f	
	1.5.1	Structure	of cellulose	10
	1.5.2	Cellulose	from NWB	11
		1.5.2(a)	Oil palm empty fruit bunch (OPEFB) fibres	12
		1.5.2(b)	Kapok seed pod (KSP) fibres	14
	1.5.3	Preparati	on of NWB cellulose hydrogels	15
		1.5.3(a)	Pretreatment of NWB	15
		1.5.3(b)	Cellulose depolymerisation	16
		1.5.3(c)	Cellulose dissolution	18
		1.5.3(d)	Cellulose crosslinking	20

1.6	Nanoe	emulsions	(NEs)	23
	1.6.1	Types of	NEs	23
	1.6.2	Compone	ents of NEs	25
		1.6.2(a)	Oils	25
		1.6.2(b)	Surfactants	25
	1.6.3	Methods	of preparation	27
		1.6.3(a)	Low-energy methods	27
		1.6.3(b)	High-energy methods	30
	1.6.4	Stability of	of NEs	34
	1.6.5	NEs for c	utaneous drug delivery	36
1.7	Toxici	ty studies f	or dermal formulations	38
1.8	Ibupro	fen (IBU) a	as a model drug	40
1.9	Proble	em stateme	ent	42
1.10	Object	tives of the	study	43
			PMENT AND CHARACTERISATION OF CELLULOSE TWO DIFFERENT NON-WOODY BIOMASS SOURCES	45
2.1	Introd	uction		45
2.2	Materi	als and me	ethods	46
	2.2.1	Materials		46
	2.2.2	Methods		47
		2.2.2(a)	Preparation of hydrolysed cellulose	47
		2.2.2(b)	Preparation of cellulose solutions	47
	2.2.3	Characte	risation of cellulose solutions	49
		2.2.3(a)	Volume of cellulose solution	49
		2.2.3(b)	Cellulose solubility and concentration solubilised cellulos	e 50
		2.2.3(c)	Index of viscosity (VI)	51
		2.2.3(d)	Microscopic analysis	52
	2.2.4	Preparati	on of cellulose hydrogels	53

		2.2.5(a)	Attenuated total reflectance-Fourier transform infrared (ATFTIR) spectroscopy	
		2.2.5(b)	Gel fraction test	.54
		2.2.5(c)	Swelling studies	.54
		2.2.5(d)	Gel strength test	.55
		2.2.5(e)	Morphology study	.56
	2.2.6	Data ana	lysis and statistics	.56
2.3	Result	ts and disc	ussion	57
	2.3.1	Characte	risation of cellulose solutions	.57
		2.3.1(a)	Preliminary study	.57
		2.3.1(b)	Investigations of chosen formulations	.59
		2.3.1(c)	Multiple regression and correlation analyses	.61
		2.3.1(d)	Viscosity study	.68
		2.3.1(e)	Microscopic analysis	.70
	2.3.2	Characte	risation of cellulose hydrogels	.72
		2.3.2(a)	Physical appearance	.72
		2.3.2(b)	ATR-FTIR spectroscopy	.75
		2.3.2(c)	pH of soaking media	.77
		2.3.2(d)	Gel fraction test	.78
		2.3.2(e)	Morphology study	.80
		2.3.2(f)	Swelling studies	.89
		2.3.2(g)	Gel strength test	.99
2.4	Concl	usions	1	02
			TION OF <i>IN VITRO</i> AND <i>IN VIVO</i> DERMAL TOXICITY OF SS CELLULOSE HYDROGELS1	
3.1	Introd	uction	1	05
3.2	Materi	als and me	ethods1	07
	3.2.1	Materials	1	107
	3.2.2	Methods	1	108

		3.2.2(a)	Preparation of cellulose hydrogels	108
		3.2.2(b)	In vitro cell viability assay	109
		3.2.2(c)	In vivo skin irritation test	111
		3.2.2(d)	In vivo skin sensitisation test	114
		3.2.2(e)	Data analysis and statistics	117
3.3	Result	ts and disc	ussion	117
	3.3.1	In vitro ce	ell viability assay	117
		3.3.1(a)	Epichlorohydrin (ECH)	117
		3.3.1(b)	Hydrogels	120
	3.3.2	<i>In vivo</i> de	ermal toxicity studies	124
		3.3.2(a)	In vivo skin irritation test	124
		3.3.2(b)	In vivo skin sensitisation test	128
3.4	Concl	usions		133
CEL	LULOS	E HYDRO	GATION OF THE POTENTIAL OF NON-WOODY BION GELS TO ACCOMODATE CATIONIC NANOEMULSIO	NS
4.1	Introd			
4.1 4.2		uction	ethods	134
		uction		134 137
	Materi	uction ials and me Materials	ethods	134 137 137
	Materi	uction ials and me Materials	ethods	134 137 137
	Materi	uction ials and me Materials Methods	ethods	134 137 137 137
	Materi	uction ials and me Materials Methods 4.2.2(a)	ethods Screening and selection of NE components	134 137 137 137 138
	Materi	uction ials and me Materials Methods 4.2.2(a) 4.2.2(b)	Screening and selection of NE components Preparation of NEs using low-energy method	134137137137138139
	Materi	uction ials and me Materials Methods 4.2.2(a) 4.2.2(b) 4.2.2(c)	Screening and selection of NE components Preparation of NEs using low-energy method Preparation of NEs using high-energy methods	134137137137138139143
	Materi	Materials Methods 4.2.2(a) 4.2.2(b) 4.2.2(c) 4.2.2(d)	Screening and selection of NE components Preparation of NEs using low-energy method	134137137137138139143144
	Materi 4.2.1 4.2.2	uction fials and me Materials Methods 4.2.2(a) 4.2.2(b) 4.2.2(c) 4.2.2(d) 4.2.2(e) 4.2.2(f) 4.2.2(g)	Screening and selection of NE components Preparation of NEs using low-energy method Preparation of NEs using high-energy methods Characterisation of NE Loading of NEs into hydrogels High performance liquid chromatography (HPLC) ar	134137137137138139143144 alysis145
	Materi 4.2.1 4.2.2	uction fials and me Materials Methods 4.2.2(a) 4.2.2(b) 4.2.2(c) 4.2.2(d) 4.2.2(e) 4.2.2(f) 4.2.2(g)	Screening and selection of NE components Preparation of NEs using low-energy method Preparation of NEs using high-energy methods Characterisation of NE Loading of NEs into hydrogels High performance liquid chromatography (HPLC) ar	134137137137138139143144 alysis145

		4.3.1(a)	Drug solubility in oils and surfactant	146
		4.3.1(b)	Optimisation of oil and surfactant compositions	147
	4.3.2	Effects of	f processing methods on NE formation	155
		4.3.2(a)	Selection of microfluidic chip	155
		4.3.2(b)	Comparisons between phase inversion composition homogenisation and microfluidisation	
	4.3.3	Morpholo	ogy study	159
	4.3.4	Stability	studies	160
		4.3.4(a)	Accelerated stability studies	161
		4.3.4(b)	Long-term stability studies	164
	4.3.5	Loading I	NE into hydrogels	168
4.4	Conclu	usions		169
_		_	TION OF <i>IN VITRO</i> DRUG RELEASE AND SKIN NOEMULSION-LOADED HYDROGELS	171
5.1	Introd	uction		171
5.2	Materi	als and me	ethods	173
	5.2.1	Materials		173
	5.2.2	Methods		173
		5.2.2(a)	Drug content study	173
		5.2.2(b)	In vitro drug release studies	174
		5.2.2(c)	In vitro skin permeation studies	176
		5.2.2(d)	HPLC analysis	177
		5.2.2(e)	Data analysis and statistics	178
5.3	Results and discussion			178
	5.3.1	Drug con	tent study	178
	5.3.2	<i>In vitro</i> di	rug release studies	180
		5.3.2(a)	NEs	180
		5.3.2(b)	Hydrogels loaded with NEs	181
		5.3.2(c)	Drug release kinetics	183

	5.3.3	<i>In v</i> itro sl	kin permeation studies	185
		5.3.3(a)	NEs	185
		5.3.3(b)	Hydrogels loaded with NEs	187
		5.3.3(c)	Mass balance studies	189
	5.3.4	Factors a	affecting drug permeation of NE-loaded hydrogels	191
5.4	Concl	usions		196
СНА	PTER 6	6 CONCLU	JSIONS AND FUTURE WORK	198
6.1	Concl	usions		198
6.2	Future	work		202
REF	ERENC	ES		205
APPENDICES				
I IST	OF PU	IRI ICATIO	ONS	

LIST OF TABLES

	Page
Table 1.1	Type of animal model used for toxicity testing (adapted from (Parasuraman et al., 2020))40
Table 1.2	Physicochemical properties of IBU41
Table 2.1	List of formulations with a volume of cellulose solution of $\geqslant 70\%60$
Table 2.2	Regression equations of MRA for the volume of cellulose solution in the preliminary study63
Table 2.3	Regression equations of MRA for the concentration of solubilised cellulose in the preliminary study63
Table 2.4	Assignment of functional groups associated with major vibration bands in FTIR spectra of cellulose
Table 2.5	Swelling kinetic parameters of hydrogels97
Table 2.6	Effects of the compositions cellulose content and alkali on the cellulose dissolution and hydrogel properties103
Table 3.1	Scoring system for skin reaction (adapted from International Organization for Standardization (ISO) (2021c))113
Table 3.2	Response categories of primary irritation index in rabbits (adapted from International Organization for Standardization (ISO) (2021c))114
Table 3.3	Magnusson and Kligman scale for grading skin reaction of guinea pigs (adapted from International Organization for Standardization (ISO) (2021a))
Table 3.4	Scoring for erythema and oedema at 24, 48 and 72 h after removal of hydrogels (n = 3)
Table 3.5	Primary irritation score and primary irritation index of hydrogels125
Table 3.6	Grading of skin sensitisation reactions for each challenge site at 24 and 48 h after removal of the hydrogels (test: $n = 10$; control: $n = 5$)129
Table 4.1	Saturated solubility of IBU in various oils and T80 surfactant147
Table 4.2	Effect of EO and T80 concentration on droplet size, PDI and zeta potential of NE formulations (n = 3, mean \pm SD)148
Table 4.3	Droplet size, PDI and zeta potential of NE formulations with and without IBU and CTAB (n = 3, mean \pm SD)152
Table 4.4	Droplet size, PDI and zeta potential of NE formulations prepared from microfluidic chips with different numbers of the upright staggered fin (n = 3, mean ± SD)

Table 4.5	Droplet size, PDI and zeta potential of NE formulations prepared from different methods (n = 3, mean \pm SD)157
Table 4.6	Drug content per weight of NE-loaded hydrogels and corresponding swelling ratio (n = 3, mean ± SD)
Table 5.1	Drug content results of NE-loaded hydrogels (n = 3, mean \pm SD)179
Table 5.2	Correlation coefficients of zero-order, first-order, Higuchi and Korsmeyer-Peppas models
Table 5.3	Drug content applied, total percentage of IBU recovery, percentage of IBU permeated and retained in the hydrogels and skin (n = 3, mean ± SD)

LIST OF FIGURES

Page	
gure 1.1 Cross-section view of human skin (created in BioRender.com; adapted from Herlihy (2017))	Figure 1.1
gure 1.2 'Bricks and mortar' model of the SC (adapted from Janssens et al (2012))	Figure 1.2
gure 1.3 Skin penetration of drug contained in hydrogels driven by a large drug concentration gradient across the skin	Figure 1.3
gure 1.4 Molecular structure of cellulose (adapted from Heinze (2016))10	Figure 1.4
gure 1.5 Lignocellulosic biomass from the plant cell wall (created in BioRender.com; adapted from Wong et al. (2021))1	Figure 1.5
gure 1.6 OPEFB and its fibres13	Figure 1.6
gure 1.7 KSP and its fibres14	Figure 1.7
gure 1.8 Common steps of hydrogel development from NWB (adapted from Wong et al. (2021))15	Figure 1.8
gure 1.9 Chemical structure of ECH (*electrophilic carbon atoms)21	Figure 1.9
gure 1.10 Proposed mechanism of crosslinking method of cellulose chains via etherification using ECH (adapted from De Miguel et al. (1999))22	Figure 1.10
gure 1.11 Structures of (A) oil-in-water, (B) water-in-oil and (C) bicontinuous NEs	Figure 1.11
gure 1.12 NE preparation methods (adapted from Sharma et al. (2022))27	Figure 1.12
gure 1.13 Changes of spontaneous curvature of surfactant occur via PIC and PIT (adapted from Chuesiang et al. (2018) and Feng et al. (2020))29	Figure 1.13
gure 1.14 Emulsion size reduction by rotor-stator homogeniser (adapted from Håkansson and Rayner (2018))31	Figure 1.14
gure 1.15 Emulsion size reduction by ultrasonication (adapted from Kumar et al (2019))32	Figure 1.15
gure 1.16 Emulsion size reduction in the (A) Y-type and (B) Z-type interaction chambers of microfluidisers (adapted from Singh et al. (2017))32	Figure 1.16
gure 1.17 Illustration of NE destabilisation through flocculation, coalescence and Ostwald ripening resulting in creaming and eventually a phase separation (adapted from Aswathanarayan and Vittal (2019))34	Figure 1.17
gure 1.18 Toxicity testing methods for dermal formulations using animal and non	Figure 1.18

Figure 2.1	Preparation of cellulose solution and hydrogel from a mixture of OPEFB and KSP cellulose49
Figure 2.2	Graph of the (A) VI measurement of cellulose solutions and (B) gel strength measurement (mechanical properties) of reswollen hydrogels
Figure 2.3	Volume of cellulose solutions prepared from different compositions of cellulose content and alkali solvent in the preliminary study $(n = 1)57$
Figure 2.4	(A) Cellulose solubility and (B) concentration of solubilised cellulose for different compositions of cellulose content and alkali solvent in the preliminary study (n = 1)
Figure 2.5	Volume of cellulose solutions prepared from different compositions of cellulose content and alkali solvent (n = 3, mean \pm SD)60
Figure 2.6	(A) Cellulose solubility and (B) concentration of solubilised cellulose for different compositions of cellulose content and alkali solvent (n = 3, mean ± SD)61
Figure 2.7	Helical cluster of NaOH, urea and water molecules around a single cellulose molecule (adapted from Wong et al. (2021))68
Figure 2.8	VI of cellulose solutions prepared from different compositions of cellulose content and alkali solvent (n = 3, mean \pm SD)69
Figure 2.9	Microscopic images of (A) OPEFB cellulose pulp, (B) KSP cellulose pulp, (C) hydrolysed OPEFB cellulose, (D) hydrolysed KSP cellulose, (E) cellulose solution for CNU482-EK21 before and (F) after centrifugation (supernatant) at a magnification of 6.3x under polarised mode71
Figure 2.10	Swollen hydrogels prepared from 2%w/v of total cellulose after soaking for ~ 2 – 3 days73
Figure 2.11	Swollen hydrogels prepared from 3%w/v of total cellulose after soaking for ~ 2 – 3 days74
Figure 2.12	Swollen hydrogels prepared from 4%w/v of total cellulose after soaking for ~ 2 – 3 days74
Figure 2.13	FTIR spectra of OPEFB pulp and cellulose, KSP pulp and cellulose and CNU282-EK21 lyophilised hydrogel75
Figure 2.14	Cellulose etherification reaction for hydrogel crosslinking (adapted from Wong et al. (2021))77
Figure 2.15	pH of soaking media for cellulose hydrogels78
Figure 2.16	Gel fraction of cellulose hydrogels prepared from different compositions of cellulose content and alkali solvent (n = 3, mean \pm SD)79
Figure 2.17	Microscopic images of lyophilised hydrogels prepared from 2%w/v of total cellulose and 6%w/v of NaOH at a magnification of 6.3x (scale bar: 100 µm)

Figure 2.18	Microscopic images of lyophilised hydrogels prepared from 2%w/v of total cellulose and 7%w/v of NaOH at a magnification of 6.3× (scale bar: 100 μm)82
Figure 2.19	Microscopic images of lyophilised hydrogels prepared from 2%w/v of total cellulose and 8%w/v of NaOH at a magnification of 6.3× (scale bar: 100 μm)
Figure 2.20	Microscopic images of lyophilised hydrogels prepared from 3% w/v of total cellulose, 6 and 7% w/v of NaOH at a magnification of $6.3\times$ (scale bar: 100 µm)84
Figure 2.21	Microscopic images of lyophilised hydrogels prepared from 3%w/v of total cellulose and 8%w/v of NaOH at a magnification of 6.3× (scale bar: 100 μm)
Figure 2.22	Microscopic images of lyophilised hydrogels prepared from 4%w/v of total cellulose and 8%w/v of NaOH at a magnification of 6.3× (scale bar: 100 μm)
Figure 2.23	Proposed structural network of cellulose hydrogels formed via chemical crosslinking with different extents of cellulose aggregation88
Figure 2.24	Swelling profiles of cellulose hydrogels prepared from $2\%w/v$ of total cellulose and $6\%w/v$ of NaOH over 72 h (n = 3, mean \pm SD)90
Figure 2.25	Swelling profiles of cellulose hydrogels prepared from $2\%w/v$ of total cellulose and $7\%w/v$ of NaOH over 72 h (n = 3, mean \pm SD)91
Figure 2.26	Swelling profiles of cellulose hydrogels prepared from $2\%w/v$ of total cellulose and $8\%w/v$ of NaOH over 72 h (n = 3, mean \pm SD)91
Figure 2.27	Swelling profiles of cellulose hydrogels prepared from $3\%w/v$ of total cellulose and 6 and $7\%w/v$ of NaOH over 72 h (n = 3, mean \pm SD)93
Figure 2.28	Swelling profiles of cellulose hydrogels prepared from $3\%w/v$ of total cellulose and $8\%w/v$ of NaOH over 72 h (n = 3, mean \pm SD)93
Figure 2.29	Swelling profiles of cellulose hydrogels prepared from $4\%w/v$ of total cellulose and $8\%w/v$ of NaOH over 72 h (n = 3, mean \pm SD)94
Figure 2.30	Gel strength of chosen hydrogels (n = 3, mean \pm SD; significant differences (ANOVA, $p < 0.05$) are indicated by different superscript letters)
Figure 2.31	Swollen hydrogels after soaking for ~ 2 - 3 days101
Figure 3.1	(A) CNU282-EK11 hydrogel formed using petri dish and (B) the corresponding oven-dried hydrogel108
Figure 3.2	Sample application sites on the back of a rabbit112
Figure 3.3	Example of the back of rabbit (A) before sample application and (B) 72 h after sample removal in an <i>in vivo</i> skin irritation test (adapted from Wang et al. (2016)). Erythema and oedema were shown at the positive

	control area (bottom left) while no skin reactions were developed at the other sample application sites113
Figure 3.4	Sample application sites during induction (weeks $1-3$) and challenge (week 5) phases on the back of a guinea pig115
Figure 3.5	Example of the back of guinea pigs in the (A) negative and (B) positive control groups in an <i>in vivo</i> skin sensitisation test (adapted from Wang et al. (2017a)). After the challenge phase, erythema and oedema were shown in the positive control application site but no changes to the negative control application site
Figure 3.6	Hs-27 cell viability results of MTT assay after incubation for 48 h with different concentrations of ECH. Experiments were carried out in 3 biological replicates with 3 technical replicates in each biological replicate (n = 9 in total, mean \pm SD; * ANOVA, $p < 0.05$)
Figure 3.7	Morphology of Hs-27 cells observed under microscope after incubation for 48 h with different concentrations of ECH at a magnification of $100 \times (\text{scale bar: } 100 \mu\text{m})$
Figure 3.8	Hs-27 cell viability of MTT assay after incubation for 48 h with different hydrogel extracts. Experiments were carried out in 3 biological replicates with 3 technical replicates in each biological replicate (n = 9 in total, mean \pm SD; * ANOVA, p < 0.05). The black dashed line indicates 70% of cell viability
Figure 3.9	Morphology of Hs-27 cells observed under microscope after incubation for 48 h with different hydrogel extracts at a magnification of 100× (scale bar: 100 μm)
Figure 3.10	Appearance of rabbit skin before application, during application and at 24, 48 and 72 h after removal of CNU282-EK11 hydrogel (C: control intact site; S: test intact site)
Figure 3.11	Appearance of rabbit skin before application, during application and at 24, 48 and 72 h after removal of CNU282-EK21 hydrogel (C: control intact site; S: test intact site)
Figure 3.12	Appearance of rabbit skin before application, during application and at 24, 48 and 72 h after removal of CNU382-EK21 hydrogel (C: control intact site; S: test intact site)
Figure 3.13	Representative pictures of the skin for sample-treated and control guinea pigs during the challenge phase at 0, 24 and 48 h after removal of CNU282-EK11 hydrogel
Figure 3.14	Representative pictures of the skin for sample-treated and control guinea pigs during the challenge phase at 0, 24 and 48 h after removal of CNU282-EK21 hydrogel
Figure 3.15	Representative pictures of the skin for sample-treated and control guinea pigs during the challenge phase at 0, 24 and 48 h after removal of CNU382-EK21 hydrogel

Figure 4.1	Stepwise optimisation of NE compositions138
Figure 4.2	Preparation of NE using PIC method
Figure 4.3	Preparation of NE using homogenisation and microfluidisation methods
Figure 4.4	Setup of microfluidisation using Texture Analyser with syringe holder and microfluidic chip141
Figure 4.5	(A) Schematic diagram of channel design, (B) 3D view of microfluidic chips with different numbers of upright staggered fin pairs, (C) enlarged view of the schematic diagram of channel design and (D) dimension of microfluidic chip.
Figure 4.6	Illustration of a negatively charged particle. The graph below displays the variation of electrical potential as a function of the distance from the surface of the charged particle (adapted from Williams (2016))151
Figure 4.7	Proposed schematic illustration of NE systems153
Figure 4.8	TEM images of (A) PIC-NE (magnification: 25000x; scale bar: 200 nm), (B) H-NE (magnification: 10000x; scale bar: 500 nm), (C) MF1-NE (magnification: 20000x; scale bar: 200 nm) and (D) MF3-NE (magnification: 25000x; scale bar: 200 nm)
Figure 4.9	(A) Formation of drug crystals in NE stored at 4°C after 2 weeks and (B) microscopic images of drug crystals in NE at magnification of 10× under polarised mode
Figure 4.10	(A) Droplet size, (B) PDI and (C) zeta potential of NEs stored at 40° C for three months during accelerated stability studies (n = 3, mean \pm SD); mth(s): month(s)
Figure 4.11	Physical appearances of NEs stored at 40°C over three months during accelerated stability studies; mth(s): month(s)163
Figure 4.12	(A) Droplet size, (B) PDI and (C) zeta potential of NEs stored at 25°C for twelve months during long-term stability studies (n = 3, mean \pm SD); mth(s): month(s)
Figure 4.13	Physical appearances of NEs stored at 25°C over twelve during long-term stability studies; mth(s): month(s)166
Figure 4.14	Proposed schematic illustration of T80 desorption from the droplet surface of NE
Figure 5.1	Franz-type diffusion cell (adapted from Alberti et al. (2017))172
Figure 5.2	Drug content study of cylindrical NE-loaded hydrogel178
Figure 5.3	G1, G2 and G3 hydrogels after swelling in NEs for 24 h180
Figure 5.4	In vitro drug release profiles of all NEs over 24 h (n = 3, mean ± SD)181

Figure 5.5	In vitro drug release profiles of NE-loaded (A) G1, (B) G2 and (C) G3 hydrogels over 24 h (n = 3, mean ± SD)
Figure 5.6	In vitro skin permeation studies of all NEs over 24 h (n = 3, mean ± SD)
Figure 5.7	In vitro skin permeation profiles of hydrogels loaded with (A) PIC-NE, (B) H-NE and (C) MF1-NE with their corresponding NEs over 24 h (n = 3, mean \pm SD; significant differences (ANOVA, p < 0.05) in the cumulative drug permeation at 24 h are indicated using different superscript letters)
Figure 5.8	Comparison of drug permeation and drug content applied192
Figure 5.9	Overview of key factors affecting drug permeation196

LIST OF ABBREVIATIONS

ANOVA Analysis of variance

ATR-FTIR Attenuated total reflectance-Fourier transform infrared

CTAB Cetyltrimethylammonium bromide
DMEM Dulbecco's Modified Eagle's Medium

DMSO Dimethyl sulfoxide

DP Degree of polymerisation

ECH Epichlorohydrin EO Ethyl oleate

FBS Fetal bovine serum

HPLC High performance liquid chromatography

IBU Ibuprofen

ICH International Council for Harmonisation

ISO International Organisation for Standardisation

KSP Kapok seed pod
LOD Limit of detection
LOQ Limit of quantification

MRA Multiple regression analysis

MTT 3-(4,5-dimethylthiazol-2-yl)-2,5-diphenyltetrazolium bromide

NaOH Sodium hydroxide
NE Nanoemulsion
NWB Non-woody biomass

OPEFB Oil palm empty fruit bunch PBS Phosphate buffered saline

PDI Polydispersity index

PIC Phase inversion composition
PIT Phase inversion temperature

SC Stratum corneum
SD Standard deviation
3D Three-dimensional

T80 Tween® 80

TEM Transmission electron microscope

VI Index of viscosity XRD X-ray diffraction

LIST OF SYMBOLS

K_a Acid dissociation constant

β Beta

cP Centipoise

R² Coefficient of determination

°C Degree celsius

g Gram h Hour L Litre

Microgram μg μL Microlitre Micrometre μm mL Millilitre Millimetre mm m۷ Millivolt min Minute mth Month Nanometre

nm Nanometre
N Newton
% Percentage

rpm Rotation per minute

s Second

cm² Square centimetre
m² Square metre
v/v Volume/volume
w/v Weight/volume
w/w Weight/weight

PEMBANGUNAN DAN PERINCIAN HIDROGEL SELULOSA BERASASKAN BIOJISIM UNTUK PENGHANTARAN UBAT NANOEMULSI KE KULIT

ABSTRAK

Hidrogel selulosa dapat berfungsi sebagai takungan ubat untuk penghantaran ubat ke kulit disebabkan ciri pengembungannya yang tinggi. Potensi hidrogel selulosa NWB pepeial sebagai platform untuk penghantaran ubat nanoemulsi (NE) ke kulit masih belum diterokai. Kajian ini bertujuan membangunkan hidrogel selulosa bagi penghantaran NE ke dalam kulit dengan melarutkan selulosa daripada tandan buah kosong kelapa sawit (E) dan kapok (K) dalam sistem alkali akueus. Sebelum pembentukan hidrogel, keterlarutan serbuk selulosa NWB (2 – 4%w/v) dengan nisbah yang berbeza (E:K: 1:1, 1:2 dan 2:1) dalam pelarut alkali dikaji dengan menggunakan berbeza kandungan natrium hidroksida (6 - 8%w/v) dan urea (2 - 6%w/v). Keterlarutan selulosa meningkat dengan kepekatan pelarut alkali dan nisbah E:K yang lebih tinggi. Pembentukan hidrogel melalui ikatan eter semasa pertautan silang terbukti daripada analisis spektroskopi inframerah bagi hidrogel kering beku. Tambahan pula, pecahan gel (~10 - 20%) hidrogel meningkat dengan kepekatan selulosa tetapi berkurangan dengan kandungan natrium hidroksida. Dengan pecahan gel yang tinggi, hidrogel juga mempunyai kekuatan gel yang tinggi tetapi ini disertai dengan nisbah pengembungan yang berkurangan. Lebih penting lagi, hidrogel yang disediakan daripada selulosa NWB campuran menunjukkan kesimbangan yang baik antara pengembungan dan kestabilan mekanikal. Seterusnya, keputusan ujian viabiliti sel in vitro, ujian perengsaan dan pemekaan kulit in vivo mengesahkan bahawa hidrogel selulosa NWB merupakan platform yang selamat untuk digunakan pada kulit. Ini menjaminkan penerokaan lebih lanjut tentang potensi hidrogel untuk penghantaran ubat ke dalam kulit. Dengan ini, NE disediakan dengan komposisi inversi fasa (PIC), penghomogenan (H) dan mikrofluidasi (MF) untuk dimuatkan ke dalam hidrogel selulosa. PIC-NE mempunyai saiz titisan yang lebih kecil (~ 33 nm) berbanding dengan H-NE dan MF-NE (~ 57 – 67 nm). Semua NE mempunyai indeks poliserakan (~ 0.25) dan keupayaan zeta (~ 24 mV) yang serupa kecuali H-NE yang mempunyai keupayaan zeta yang lebih rendah (~ 19 mV). Kajian kandungan ubat menunjukkan bahawa hidrogel dapat menampung NE yang mengandungi ubat (1300 – 4000 μg/g). Pelepasan ubat daripada hidrogel selulosa yang dimuatkan dengan NE mengambil ~ 3 kali lebih lama daripada NE sahaja bagi mencapai penara. Namun begitu, peresapan kulit *in vitro* hidrogel selulosa yang dimuatkan dengan NE (~ 8 – 30 μg/cm²) adalah lebih tinggi daripada NE sahaja (~ 11 – 21 μg/cm²). Tambahan pula, PIC-NE mencapai kadar peresapan ubat yang lebih tinggi daripada NE lain dan juga semasa dimuatkan dalam hidrogel selulosa. Kesimpulannya, hidrogel selulosa NWB yang disediakan daripada dua sumber biojisim berbeza berpotensi untuk digunakan sebagai platform yang selamat dan efektive bagi penghantaran NE ke kulit.

DEVELOPMENT AND CHARACTERISATION OF BIOMASS-BASED CELLULOSE HYDROGELS FOR NANOEMULSION DRUG DELIVERY TO THE SKIN

ABSTRACT

Cellulose hydrogels with a substantial swelling ability can serve as drug reservoirs for drug delivery to the skin. The potential of solid non-woody biomass (NWB) cellulose hydrogels as a platform for nanoemulsion (NE) drug delivery to the skin remains unexplored. This study aims to develop NWB cellulose hydrogels for dermal delivery of NE by dissolving cellulose from oil palm empty fruit bunch (E) and kapok seed pod (K) fibres in an aqueous alkali solvent system. Prior to hydrogel preparation, solubilisation of NWB cellulose powder (2 – 4%w/v) with varying ratios (E:K: 1:1, 1:2 and 2:1) in alkali solvents composed of different concentrations of sodium hydroxide (6 – 8%w/v) and urea (2 – 6%w/v) was examined. Increasing total alkali concentration and the E:K ratio enhanced cellulose solubilisation. The formation of hydrogel through ether bond during crosslinking was evident from the infrared spectroscopic analysis of lyophilised hydrogels. Additionally, gel fraction (~10 – 20%) of hydrogels increased with cellulose concentration but decreased with sodium hydroxide concentration. With a high gel fraction, the hydrogels also have a high gel strength but this was accompanied by a reduced swelling ratio. More importantly, hydrogels prepared from mixed NWB cellulose exhibited a well-balanced swelling and mechanical stability. Subsequently, in vitro cell viability study, in vivo skin irritation and sensitisation studies confirmed that NWB cellulose hydrogels are a safe platform for use on the skin, assuring the further exploration of hydrogel potential for dermal drug delivery. Following this, NEs were prepared using phase inversion composition (PIC), homogenisation (H) and microfluidisation (MF) for loading into hydrogels. PIC-NE possessed a smaller droplet size (~ 33 nm) than H-NE and MF-NE (~ 57 – 67 nm). All NEs showed similar polydispersity index (\sim 0.25) and zeta potential (\sim 24 mV) values, except for H-NE with a lower zeta potential (\sim 19 mV). Drug content study revealed that hydrogels could accommodate drug-loaded NEs (1300 - 4000 μ g/g). The drug release from NE-loaded hydrogels took \sim 3 times longer time than NEs alone to reach a plateau. Interestingly, *in vitro* drug permeation was generally higher with NE-loaded hydrogels (\sim 8 - 30 μ g/cm²) than NEs alone (\sim 11 - 21 μ g/cm²). Furthermore, PIC-NE achieved a higher drug permeation than the other NEs, even when they were loaded in hydrogels. In conclusion, NWB cellulose hydrogels prepared from two different biomass sources hold great promise as a safe and effective dermal delivery platform for NEs.

CHAPTER 1

INTRODUCTION

1.1 Overview

Cutaneous drug delivery refers to a route of drug administration into the skin that aims for systemic (transdermal drug delivery) or local action (topical drug delivery) (Benson, 2012; Kathe and Kathpalia, 2017). This delivery route is attractive mainly because of the advantages of avoiding the hepatic first-pass metabolism, the potential to reduce frequency of administration and a better patient medication compliance (Souto et al., 2022).

Generally, hydrogels are designed to hold enormous amount of drugs to enhance drug penetration into the skin by establishing a high drug concentration gradient across the skin (Chen et al., 2006; Hoare and Kohane, 2008; Cascone and Lamberti, 2020). To date, hydrogels are commonly prepared from synthetic polymers or commercial cellulose derivatives such as polyvinyl alcohol, polyacrylic acid, hydroxypropylmethyl cellulose and carboxymethyl cellulose (Ahmed, 2015; Navarra et al., 2015; Cascone and Lamberti, 2020).

Hydrogels developed from natural sources, especially native cellulose can be a promising drug delivery platform due to their high biocompatibility. Owing to the abundant hydroxyl groups within cellulose chains, fabrication of cellulose hydrogels becomes feasible by crosslinking these cellulose chains through either chemical or physical methods. The application of cellulose hydrogels prepared from natural resources is often limited due to their poor mechanical properties and stability (Rawat Singh et al., 2015; Wong et al., 2023). In achieving successful drug delivery into the skin, both swelling and mechanical properties of hydrogels are usually given more focus during cellulose hydrogel development (Chang and Zhang, 2011; Ciolacu et al., 2016; Kabir et al., 2018).

Cellulose from non-woody biomass (NWB) represents a largely untapped cellulose reservoir with great potential for cellulose hydrogel development. The limited wood supply has spurred interest in using NWB as an alternative renewable source for hydrogel production from native cellulose. For the creation of cellulose hydrogels for dermal drug delivery, comprehensive research encompassing optimisation, toxicity evaluation and efficiency testing is crucial.

Overall, this chapter provides a basic overview of skin structure and cutaneous drug delivery. In addition, this chapter also delves into the context and comprehension related to the development of cellulose hydrogels from native cellulose and nanoemulsions (NEs) for cutaneous drug delivery, along with exploring skin toxicity studies and the utilisation of ibuprofen (IBU) as a model drug.

1.2 Human skin

Human skin is the largest organ of the body that covers the body surface area of approximately 1.7 m² (Benson, 2012; Parihar et al., 2020). Our skin is commonly known as a barrier to the environment that prevents the invasion of the chemical allergens and microorganisms as well as protects us against the ultraviolet radiation injuries and the loss of moisture or body nutrients (Vitorino et al., 2015).

Basically, the skin comprises three main layers: subcutaneous tissue, dermis and epidermis (Figure 1.1) (Herlihy, 2017). Subcutaneous tissue is the innermost skin layer which consists of fat and connective tissues. This skin layer is a vital heat insulator that helps to regulate our body temperature (Gregory, 1989; Park et al., 2022). The dermis is a layer sandwiched between the epidermis and underlying subcutaneous tissue. This layer mainly consists of collagen fibrils and connective tissue embedded within a mucopolysaccharide matrix (Benson, 2012; Hmingthansanga et al., 2022). The collagen fibrils give mechanical strength to the skin while the connective tissue provides skin elasticity and flexibility. Fibroblasts

produce the extracellular matrix components of the connective tissue such as collagens, glycosaminoglycans and proteoglycans while immune cells (e.g. mast cells and macrophages) are the predominant cell types in the matrix that produce an immune and inflammatory response. In addition, the dermis is furnished with blood lymphs, nerve endings, hair follicles, sebaceous and sweat glands that extended to the dermal side of the dermo-epidermal junction. The blood vascular network in the dermis allows the delivery of nutrients and oxygen to as well as the removal of wastes from the skin tissues (Ng and Lau, 2015).

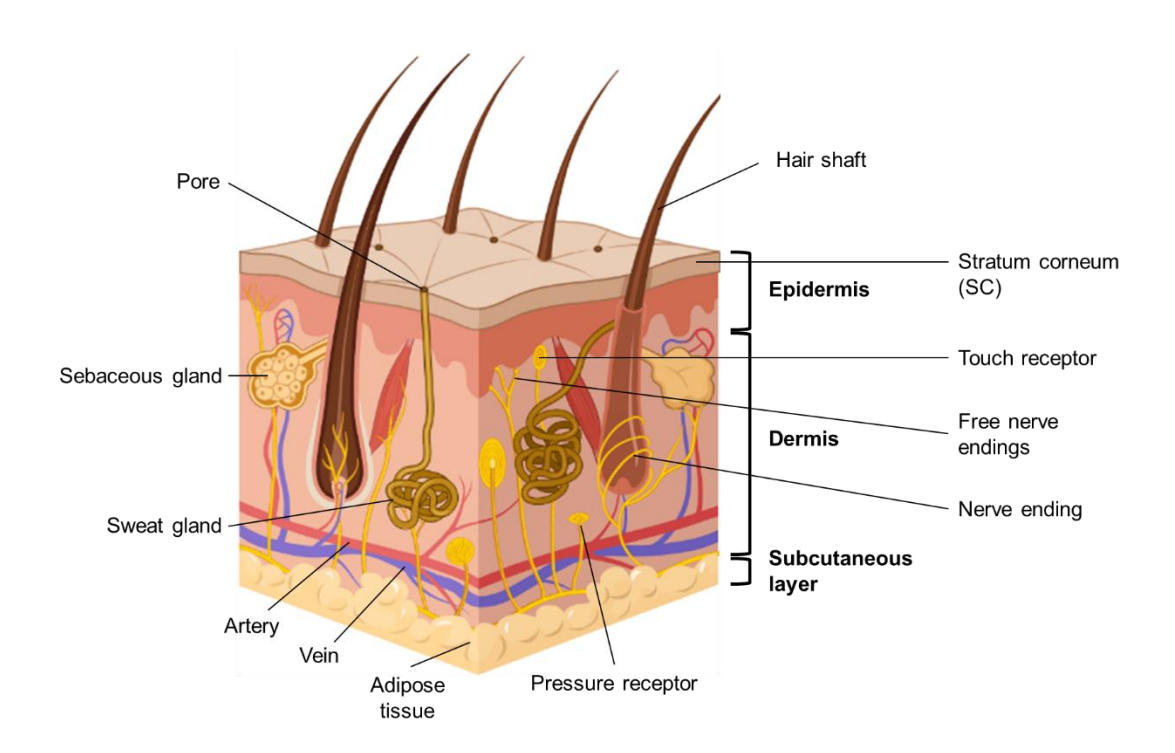


Figure 1.1 Cross-section view of human skin (created in BioRender.com; adapted from Herlihy (2017))

The epidermis is a thin outer layer of the skin and can be divided into several anatomical layers depending on the differentiation stages (Walters and Roberts, 2002; Hmingthansanga et al., 2022). The structure of the keratinocytes changes from the bottommost layer – stratum basale, then to the stratum spinosum, stratum ganulosum, stratum lucidum and finally to the outermost stratum corneum (SC). During the maturation process, different proteins and lipids are synthesised and

expressed by keratinocytes. Upon differentiation, the cells become enucleated and flattened, which are also known as non-viable corneocytes. The corneocytes are composed mainly of 70 – 80% of keratin protein and 20% of lipids within the cornified cell envelope (Benson, 2012). The SC organisation has been described as the 'bricks and mortar' model (Figure 1.2) (Janssens et al., 2012; Hmingthansanga et al., 2022). The brick wall-like structure of the corneocytes represents the 'bricks' in a 'mortar' of intercellular lipids with desmosomes acting as molecular rivets between the corneocytes. The intercellular lipids of SC are known as lipid lamellae which is made up of ceramides, cholesterol and free fatty acids (Michaels et al., 1975; Nemes and Steinert, 1999; Janssens et al., 2012; Gorzelanny et al., 2020).

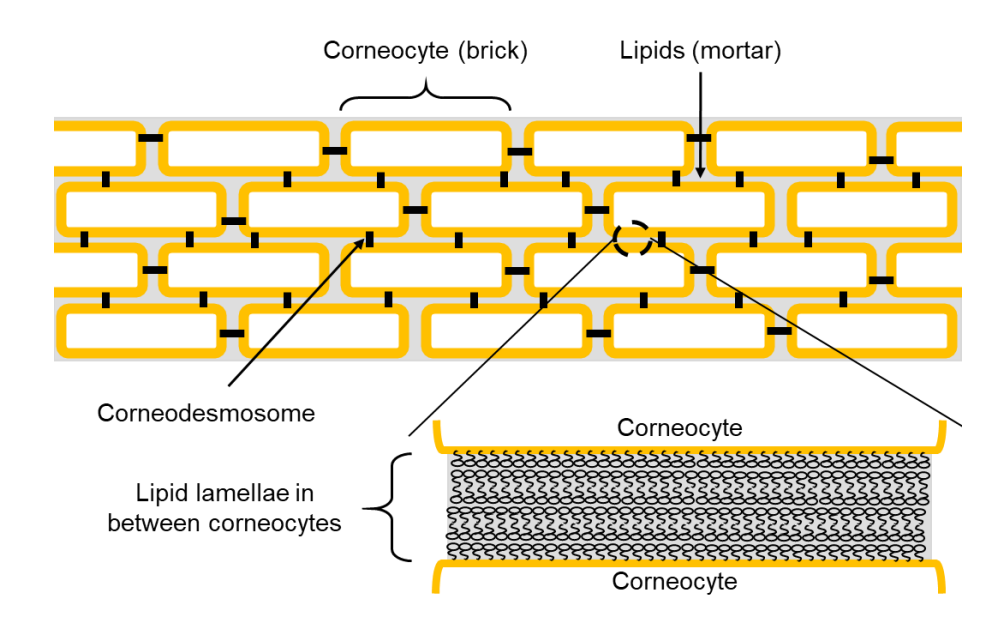


Figure 1.2 'Bricks and mortar' model of the SC (adapted from Janssens et al. (2012))

Despite the skin is readily accessible and an ideal site for the administration of therapeutic compounds for local (topical) and systemic (transdermal) effects, the SC is the principal barrier for the permeation of drugs (Benson, 2005; Vitorino et al., 2015; Gorzelanny et al., 2020). The low drug permeability of the SC is mainly attributed to the arrangement of corneccytes within the interspersed lipids ('bricks and

mortar') (Benson, 2005; Haltner-Ukomadu et al., 2019). Overcoming this barrier is one of the major challenges for the effective delivery of drugs to the skin.

1.3 Cutaneous drug delivery

There are two ways for active compounds to be administrated through the skin – topical and transdermal routes (Kathe and Kathpalia, 2017). Topical route allows the actives to penetrate the deeper regions of the skin for the local action. While transdermal absorption of drugs targets the drug delivery to the systemic circulation and eventually exerts the effect to the specific organs or body sites.

Cutaneous drug delivery is advantageous over oral administration route due to the flexibility of terminating drug administration, avoidance of the first-pass metabolism and undesirable systemic side effects in patients (e.g. adverse gastrointestinal effects) (Benson, 2012; Sadab et al., 2022). Nevertheless, the unique physicochemical composition and architecture of the SC are the main factor to cause poor absorption of drugs through the skin. Therefore, drugs that exhibit specific physicochemical properties such as partition coefficient (log P) of $\sim 1 - 3$, molecular weight lower than 500 Dalton and melting point less than 200°C are favourable candidates for skin drug delivery (Hadgraft, 2004; Chen and Gao, 2016; Chatterjee et al., 2022).

Formulation designs are often required to improve the delivery of drugs into the skin, even though the drug fulfills the favoured physicochemical criteria for skin delivery (Walters and Roberts, 2002; Herbig et al., 2023). The enhancement strategies including active and passive methods rely on two main approaches: increasing skin permeability and/or thermodynamic activity of the drug in formulations (Vitorino et al., 2015). Passive penetration enhancement can be achieved by increasing the drug's thermodynamic activity in formulations (e.g. supersaturated and nanocarrier) or using solvents as skin penetration enhancers to interact with the skin

constituents (lipids and proteins) to promote drug permeation (Lane et al., 2012). The passive method is relatively cheap as compared to the active methods because no specific equipment is required. Still, this technique is mostly limited to drugs with small molecular weight (< 500 Dalton) and may irritate the skin due to high concentration of chemical solvents (Ramadon et al., 2022).

On the other hand, active penetration enhancement involves the use of external energy to act as a driving force and/or to induce physical manipulations to the SC (Vitorino et al., 2015). The active methods rely on applying various forms of energy (e.g. heat, sound, electrical and magnetic) or weakening the SC barrier by mechanical means (e.g. microneedles). This allows more drugs to be delivered through the skin, especially for drugs with high molecular weight (> 500 Dalton) and hydrophilicity. However, the application of active methods is usually costly due to the requirement of external instrument and a sophisticated manufacturing process (Ramadon et al., 2022).

1.4 Hydrogels

Hydrogels are crosslinked networks of hydrophilic polymers that can swell substantially but resist dissolution in an aqueous medium (Hoare and Kohane, 2008; Kabir et al., 2018). Additionally, hydrogels can be formulated in different physical forms including films, slabs, microparticles, nanoparticles and coatings. Researchers have been focusing on hydrogels for diverse fields such as biomedical engineering, biomaterials, water purification and even agriculture due to their biocompatibility, biodegradability and tunable properties (Birajdar et al., 2021; Bercea, 2022). The crosslinking density, porosity, swelling properties and mechanical strength of hydrogels can be tuned by varying the components (e.g. crosslinkers, polymers and solvents) and preparation methods to exhibit desired characteristics (Wong et al., 2021; Zainal et al., 2021). These unique properties make hydrogels highly valuable in

various applications including medical implants, contact lenses, personal care products and wound dressing (Ahmed, 2015).

1.4.1 Types of polymers

Hydrogels can be formulated from synthetic, natural or hybrid combinations of polymers. Most hydrogels marketed today are produced from synthetic polymers (e.g. polyvinyl alcohol, polyacrylic acid and polyethylene glycol) derived from non-renewable petrochemicals due to the ease of synthesis (Ahmed, 2015; Navarra et al., 2015; Cascone and Lamberti, 2020). Hydrogels fabricated from synthetic polymers also show promising properties suitable for their applications. For instance, the first hydrogel material crosslinked with formaldehyde and marketed as a biomedical implant under the trade name of Ivalon® was polyvinyl alcohol (Rizwan et al., 2017). Hydrogels produced from polyvinyl alcohol usually exhibit low toxicity, good biocompatibility, high water absorption capacity and good mechanical properties (Wang et al., 2021). While, polyacrylic acid is ideal for producing pH-responsive hydrogel systems due to the presence of carboxylic acid functional groups (Ishak et al., 2020). Hydrogels made from polyethylene glycol are applied for biological applications including cell scaffolds and drug delivery due to their anti-fouling, non-immunogenic and good biocompatibility properties (Zhu, 2010; Chang et al., 2017).

On the other hand, natural polymers are greener alternatives and are preferred over synthetic ones due to low cost, better biodegradability, wide availability and non-toxicity (Varghese et al., 2020). Natural polymers such as polypeptides (e.g. collagen and gelatin) and polysaccharides (e.g. starch, lignin, alginate, chitosan, hyaluronic acid, carrageenan and cellulose) are commonly used to create hydrogels. Yet, most natural hydrogels possess poor mechanical properties that can limit their intended applications (Varghese et al., 2020; Wang et al., 2022). The incorporation of reinforcing agents including cellulose nanocrystals (Olad et al., 2020), natural rubber

(Srirachya et al., 2018), silica (Boonmahitthisud et al., 2017) and clay materials (Dai and Huang, 2017) has been employed to improve the mechanical properties of natural hydrogels. It is also proposed that hybrid hydrogels prepared by blending natural and synthetic polymers can merge the advantages of both polymers (Bao et al., 2019). The resulting hybrid hydrogels can exhibit improved properties, especially thermal stability, biodegradability, biocompatibility, swelling and mechanical properties (Chen et al., 2015; Fan et al., 2021). For instance, Chen et al. (2015) reported that hydrogels consisting of sugarcane bagasse cellulose, carboxymethyl cellulose and poly(N-isopropylacrylamide) exhibited higher mechanical strength and swelling ability than pure sugarcane bagasse cellulose hydrogels.

1.4.2 Crosslinking of hydrogels

Crosslinking is crucial to establish hydrogel network structure and retain structure while swelling. Hydrogel crosslinking can be attained mainly through two main approaches: physical or chemical crosslinking of polymer chains (Zhang and Huang, 2012; Khan et al., 2016). Physical crosslinking involves chain entanglement and high structural cohesion because of reversible intermolecular interactions without using crosslinkers. Physical crosslinking methods such as freeze-thawing, forming ionic interactions or hydrogen bonds are the most common methods used to form hydrogels (Khan et al., 2016; Shoukat et al., 2021). While chemical crosslinking occurs by forming covalent bonds between polymer chains, resulting in a permanent hydrogel network. The covalent bonds can be formed by reactions between activated functional groups of polymer chains, small molecular weight crosslinkers, free radical polymerisation reactions or enzymatic reactions (Khan et al., 2016; Shoukat et al., 2021).

Physical crosslinking is often easier than chemical crosslinking and does not require hazardous reagents like crosslinkers (Shoukat et al., 2021). However,

physical hydrogels are more prone to degradation, particularly in high-stress conditions due to the fluctuations in pH, temperature and ionic strength. In contrast, most chemical crosslinked hydrogels exhibit superior mechanical properties and stability as compared to the physical crosslinked hydrogels.

1.4.3 Hydrogels for cutaneous drug delivery

Hydrogels show promise as a platform for dermal drug delivery owing to their high swelling ability. They can act as a large drug depot with a high drug thermodynamic activity, facilitating drug delivery to the skin. This is accomplished by improving the passive flux across the skin due to a large drug concentration gradient created (Figure 1.3) (Chen et al., 2006; Hoare and Kohane, 2008; Coneac et al., 2015).

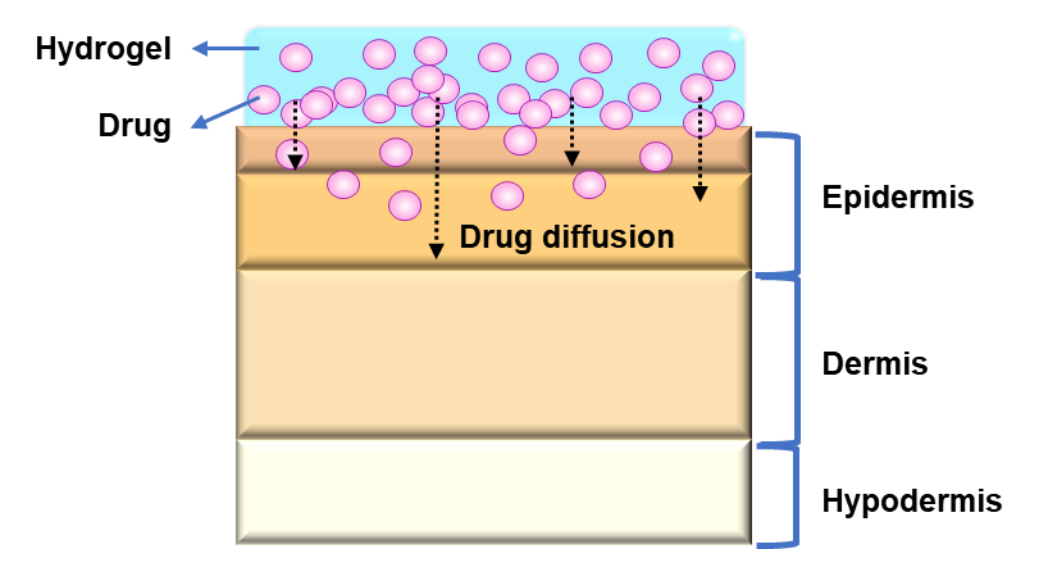


Figure 1.3 Skin penetration of drug contained in hydrogels driven by a large drug concentration gradient across the skin

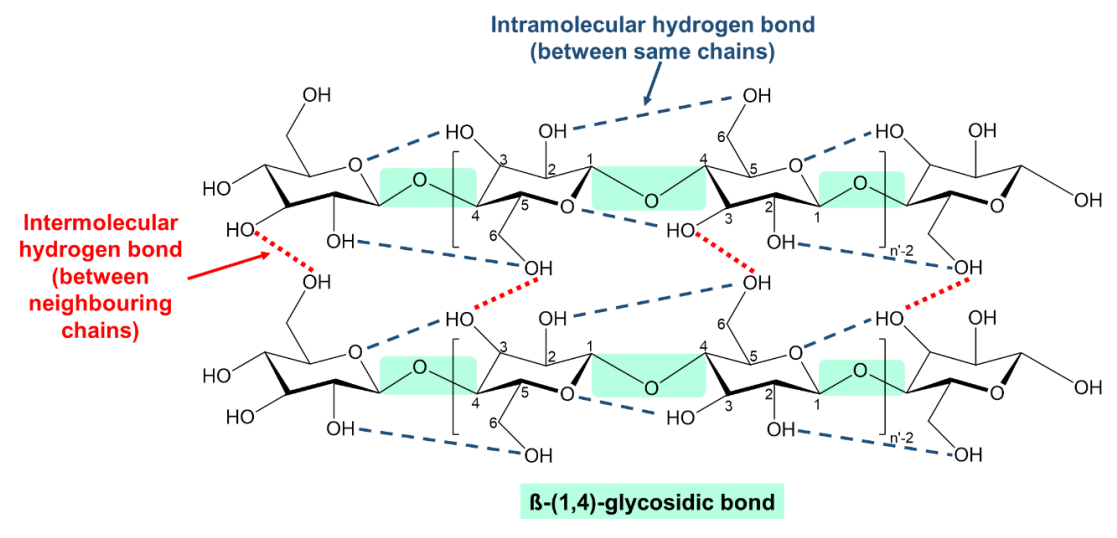
Hydrogels can do more than just carry simple solvent systems. They can also be a carrier for novel formulations like nanoparticles, NEs, microemulsions and liposomes (Almoshari, 2022). Hydrogels can increase drug penetration into the skin by prolonging the residence time of these novel formulations on the skin (Arancibia et

al., 2016). Besides, it is possible to tune the drug release manner of hydrogels by regulating the crosslinking density of hydrogels (Briggs et al., 2022). Hydrogels' occlusion and hydration effects may also be crucial for enhanced dermal drug delivery (Warner et al., 2003; Benson, 2005; Ribeiro et al., 2018; Vaz et al., 2019).

1.5 Non-woody biomass (NWB) cellulose as a source of biopolymer for hydrogel fabrication

1.5.1 Structure of cellulose

Cellulose is made up of a long chain of glucose monomers joined together through β -(1, 4)-glycosidic linkage as shown in Figure 1.4 (Heinze, 2016). Taking advantage of the abundant hydroxyl groups present on cellulosic chains, an extensive three-dimensional (3D) network of hydrogels can be easily achieved by establishing intermolecular hydrogen bonding within the cellulosic chains and/or covalent bonding with functionalised crosslinkers (Chang and Zhang, 2011; Wong et al., 2021).



n' = repeating unit of cellobiose where n' = 0.5 × degree of polymerisation

Figure 1.4 Molecular structure of cellulose (adapted from Heinze (2016))

1.5.2 Cellulose from NWB

Cellulose is known as the most abundant natural biopolymer on the Earth, mainly derived from the plant cell wall and also other sources including certain bacteria and fungi (Praveen Kumar et al., 2019). Lignocellulosic biomass is a major constituent of the plant cell wall, consisting of 40 – 50% of cellulose, 25 – 30% of hemicellulose and 15 – 20% of lignin (Figure 1.5) (Tayyab et al., 2017; Jędrzejczyk et al., 2019). The composition of cell walls varies widely among species and within an individual, depending on the cell type or plant response to environmental conditions (Sorek et al., 2014). In nature, cellulose is embedded within the lignin and hemicellulose matrix to give a supporting strength to the plant cell wall (Tayyab et al., 2017). In addition to its abundance, cellulose possesses attractive properties such as non-toxic, biodegradable and biocompatible, making it a promising alternative to synthetic polymers (Ma et al., 2015).

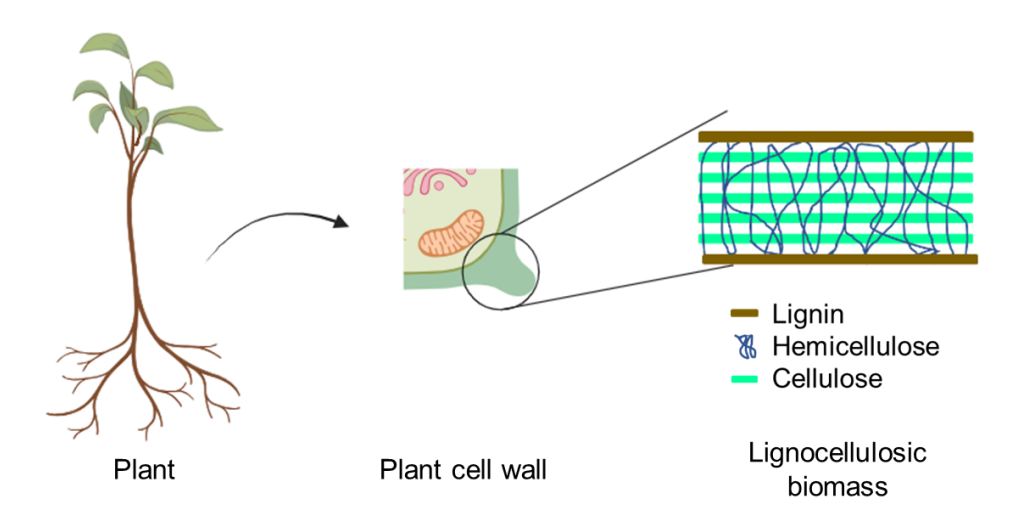


Figure 1.5 Lignocellulosic biomass from the plant cell wall (created in BioRender.com; adapted from Wong et al. (2021))

Lignocellulosic biomass can be classified into woody biomass (WB) and NWB. Nowadays, commercial cellulose derivatives (e.g. cellulose esters and ethers) is mainly produced from dissolving pulps with a high alpha cellulose content (> 90%), a relatively low hemicellulose content (< 3%) and a very low lignin content (< 0.05%)

(Harsono et al., 2016). Dissolving pulps are primarily produced from wood pulps (85 – 88%) and naturally highly pure cellulose sources such as cotton linters (12 – 15%) (Klemm et al., 2005; Chen et al., 2016; Heinze et al., 2018b). Nevertheless, the supply of wood is limited mainly due to poor forest management, high market demand, uncontrolled wood fuel production and lumbering (Alhassan et al., 2023). Considering the issues of the heavy reliance on wood resources and the depletion of wood, cellulose from NWB is introduced as an alternative raw material to produce dissolving pulps (Chen et al., 2016; Azeez, 2018).

Typically, NWB can be categorised into agricultural residues, native plants and natural non-wood plant fibres (Tye et al., 2016). NWB is suggested as an alternative native cellulose source because of its widespread availability, low cost, ease to process as well as having a short growth and harvest period (Tye et al., 2016; Abd El-Sayed et al., 2020). In addition, NWB such as flax, sisal, hemp, kapok and ramie has a higher cellulose content (~ 70%) than WB (40 – 50%) (Hon, 1996). NWB with a lower lignin content requires less chemical treatment during the cellulose extraction process, specifically delignification (Tye et al., 2016).

1.5.2(a) Oil palm empty fruit bunch (OPEFB) fibres

Malaysia is a leading palm oil producer in the world, ranking second in production (Padzil et al., 2020). The oil palm plantations and mills generate substantial amounts of agricultural wastes including oil palm trunks (~ 5%), oil palm fronds (~ 37%), OPEFB (~ 10%), palm kernel shells (~ 3%), mesocarp fibres (~ 5%) and palm oil mill effluent (~ 27%) (Padzil et al., 2020; Yeo et al., 2020). According to the Economics and Industry Development Division of the Malaysian Palm Oil Board, palm oil industries in Malaysia produced ~ 50 million tonnes of palm oil in 2023 (Economics and Industry Development Division - Malaysian Palm Oil Board, 2024). For each tonne of palm oil produced, ~ 1.07 tonnes of OPEFB can be produced (Dolah et al.,

2021). OPEFB is obtained from the empty stalks of fresh fruit bunches after the separation of oil palm fruits (Figure 1.6). Meanwhile, OPEFB strand fibres are acquired through a sequence of fibre extraction processes from OPEFB. Traditionally, OPEFB is utilised as a fuel for steam generation in palm oil mills and the resulting ash is used as an organic fertiliser (Anyaoha et al., 2018). However, the combustion of OPEFB is strongly discouraged due to the emission of greenhouse gases, contributing to the global climate change phenomenon (Dolah et al., 2021). Moreover, constraints such as labour expenses, high weight and volume to nutrient content ratio and pest attraction are factors restricting the use of OPEFB as both mulch and organic fertilisers (Anyaoha et al., 2018). Therefore, OPEFB are valorised for other value-added applications to reduce its environmental footprint, including composting, production of medium density fiberboard and paper manufacturing (Dolah et al., 2021). In view of the high cellulose content of 56% in its fibres, OPEFB can be utilised as an alternative source of cellulose for producing dissolving pulps to reduce waste generated (Harsono et al., 2016; Tye et al., 2017).



Figure 1.6 OPEFB and its fibres

1.5.2(b) Kapok seed pod (KSP) fibres

KSP fibres are natural non-woody fibres obtained from the seed pods of the kapok (*Ceiba pentandra* (L.) Gaertn.) tree (Tye et al., 2012; Baraniak and Kania-Dobrowolska, 2023). KSP fibres are silky, light-weight, yellowish and cotton-like fibre (Figure 1.7). Owing to its hydrophobic (waxy surface), oleophilic and biodegradable properties, KSP fibres are primarily used as a stuffing material for pillows, cushions and mattresses in Malaysia (Chan et al., 2022; Baraniak and Kania-Dobrowolska, 2023). However, the market growth of KSP fibres is hampered by the difficulty of spinning them into yarns and the introduction of synthetic substitutes such as polyester fibres. From 2001 to 2021, the global production of KSP fibres decreased by almost half to ~ 75000 tonnes (Food and Agriculture Organization of the United Nations, 2024). Hence, researchers have started to explore the potential use of KSP fibres such as reinforcement fibre for recycled paper, oil-water separation, dye adsorption and wastewater treatment (Leh et al., 2021; Wang et al., 2023). KSP fibres consist of 50% cellulose and are also identified as a potential cellulose source for dissolving pulp production (Tye et al., 2015; Tye et al., 2017).



Kapok seed pod (KSP)



Kapok seed pod (KSP) fibres

Figure 1.7 KSP and its fibres

1.5.3 Preparation of NWB cellulose hydrogels

The development of cellulose hydrogels from NWB involves several steps, namely pretreatment of biomass, cellulose dissolution and crosslinking as summarised in Figure 1.8 (Wong et al., 2021). Notably, using low-purity cellulose can result in low production efficiency, high manufacturing cost, poor product quality and increased environmental pollution (Chen et al., 2016; Vilajuana, 2016). Therefore, the production of dissolving pulp from NWB is particularly important to minimise the adverse effects of impurities on the accessibility of cellulose hydroxyl groups to the reacting chemicals. Subsequently, the steps involved in preparing native NWB cellulose hydrogels can vary depending on the types of solvents and crosslinking methods used.

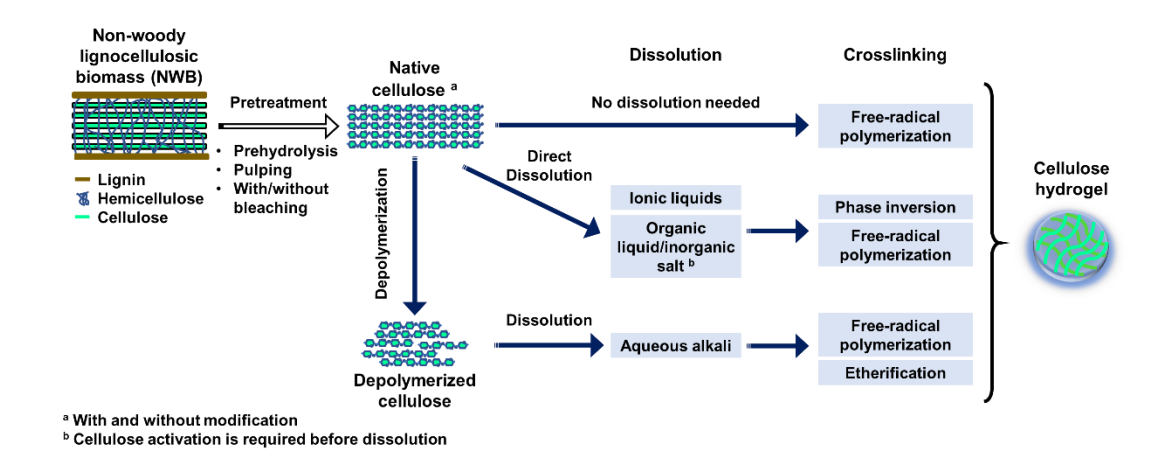


Figure 1.8 Common steps of hydrogel development from NWB (adapted from Wong et al. (2021))

1.5.3(a) Pretreatment of NWB

Similar to WB, pretreatment is required to extract dissolving pulp from other components in NWB. The parameters of pretreatment processes can be specific for different sources or compositions of biomasses. As mentioned earlier, non-wood fibres with more cellulose and less lignin content usually require less harsh chemicals and processing conditions (Azeez, 2018).

Generally, pretreatment involves prehydrolysis, pulping and optional bleaching (Heinze et al., 2018b). Prehydrolysis facilitates cellulose extraction by removing hemicellulose, loosening the pulp matrix and improving the accessibility of lignin to subsequent pulping and bleaching chemicals (Wan Rosli et al., 2004; Heinze et al., 2018b). Various methods can be carried out for prehydrolysis including hot water treatment, autohydrolysis, acidic or alkaline medium and steaming (Kumar and Christopher, 2017). This is followed by the pulping process which helps the removal of most lignin through mechanical, thermal, semi-chemical or wholly chemical methods (Azeez, 2018). The chemical soda pulping (sulphur-free) process is wellsuited for NWB with low lignin content and appears to be a better technique due to its efficacy and environmental friendliness as compared to other sulphur-containing processes (e.g. sulphite and Kraft processes) (Wan Daud et al., 2003). Finally, the residual lignin in the pulp can be removed through bleaching processes such as chlorination and oxidation to yield high-purity cellulose (Azeez, 2018). The removal of residual lignin is optional and depends on the usage of final products. Particularly for paper production, bleaching is required to improve the brightness of the products (Azeez, 2018). Additionally, the use of high purity cellulose can improve the transparency of cellulose-based products such as cellulose films, membranes or other materials where optical clarity is a key requirement (Zhu et al., 2017; Farid et al., 2022).

1.5.3(b) Cellulose depolymerisation

Cellulose depolymerisation refers to the process of reducing the molecular weight (degree of polymerisation (DP)) of cellulose (Driscoll et al., 2009; Malešič et al., 2021). It is worth stressing that the DP of cellulose is highly related to cellulose dissolution, with high DP cellulose commonly resulting in low dissolution (Wong et al., 2021). Therefore, cellulose from NWB likes wheat straw and bagasse can achieve a

direct dissolution in a given system due to their lower DP (~ 1000) as compared to the WB (4000 – 5500) (Hallac and Ragauskas, 2011). Despite this, mild depolymerisation may still be necessary to improve cellulose dissolution in solvents with low dissolution ability, especially for aqueous alkali solvents (Budtova and Navard, 2016; Wong et al., 2021).

Cellulose depolymerisation can be accomplished through several techniques that can be classified as physical, chemical and physiochemical methods (Wong et al., 2021). Physical methods require a substantial amount of energy to reduce particle size and increase the specific surface area of cellulose (Jędrzejczyk et al., 2019; Wong et al., 2021). For instance, electron beam irradiation was utilised to degrade kenaf core cellulose pulp (Mohammad Padzil et al., 2018). During electron beam irradiation, unstable macroradicals are generated through the direct transfer of energy from electrons to cellulose molecules (Mohammad Padzil et al., 2018). The formation of radicals especially on carbon-1 and carbon-4 of cellulose can result in the breaking of glycosidic bonds (Wong et al., 2021). Physical methods are generally considered environmentally friendly as they do not involve chemicals.

Acid hydrolysis is the most commonly used chemical method in which the glycosidic bonds in the amorphous regions of cellulose can be cleaved by the hydronium ions (de Souza Lima and Borsali, 2004; Almashhadani et al., 2022). The individual crystallites are released upon bond cleaving and further broken down into a lower DP. Sulphuric acid is preferred over hydrochloric acid for depolymerisation due to the formation of a sulphate-coated cellulose complex via the esterification of hydroxyl groups of cellulose by sulphate ions (Bondeson et al., 2006; Ng et al., 2021). This leads to the repulsion between the hydrolysed cellulose with negatively charged surfaces, enhancing the stability of hydrolysed cellulose dispersion (Lu and Hsieh, 2010; Ma et al., 2015). Unlike sulphuric acid, hydrochloric acid-treated cellulose can reaggregate by forming hydrogen bonds between the hydroxyl groups of cellulose chains (Araki et al., 1998; Ma et al., 2015; Wu et al., 2023).

Physiochemical methods combine both physical and chemical processes. Autohydrolysis is an example of a physiochemical method where cellulose is treated with water at a high temperature (> 150°C) and pressure (Jędrzejczyk et al., 2019). This process can result in more autoionisation of water into acidic hydronium ions, increasing acid hydrolysis of the glycosidic bonds of cellulose (Wong et al., 2021). This method has been employed to depolymerise cellulose pulps from OPEFB up to ~20% and kenaf core up to ~40% at a relatively mild condition (100 – 140°C) (Gan et al., 2016; Gan et al., 2017b).

1.5.3(c) Cellulose dissolution

Cellulose has poor solubility in common solvent systems (e.g. water and ethanol) because of the extensive inter- and intramolecular hydrogen bondings in the structure (Richardson and Gorton, 2003; Chang and Zhang, 2011; Chami Khazraji and Robert, 2013; Wong et al., 2021). Therefore, efforts to discover solvents to dissolve cellulose have been devoted for a few decades. These solvents can be broadly classified into derivatising and non-derivatising solvents (Medronho and Lindman, 2014).

Derivatising solvents (e.g. carbon disulphide and N-methylmorpholine N-oxide monohydrate) chemically modify the cellulose structure through processes such as esterification, etherification, nitration and xanthation. The hydroxyl groups of cellulose derivatives are partially or totally substituted by functional groups such as methyl, hydroxypropyl or carboxylmethyl groups. This modification can reduce the formation of hydrogen bonds within cellulose molecules and improve cellulose dissolution (Chang and Zhang, 2011; Lavinia et al., 2016; Kabir et al., 2018). While these solvents have a high dissolution power, they are associated with some drawbacks such as volatility, toxicity due to the release of harmful gaseous and high cost (Jin et al., 2007; Zhang et al., 2010; Zhang et al., 2018). For example, the conventional viscose

manufacturing process employs hazardous and expensive carbon disulphide which can generate harmful byproducts such as hydrogen disulphide, sulphur dioxide and carbonyl sulphide (Kumar and Christopher, 2017; Sayyed et al., 2019). Whereas, N-methylmorpholine N-oxide monohydrate/water system is an environmentally-friendly alternative that has been commercially adopted for the production of Lyocell™ fibres, yet effective recovery processes are required for the retrieval of this costly solvent (Jin et al., 2007; Zhang et al., 2010; Sayyed et al., 2020). Therefore, derivatising solvents are rarely reported in preparing cellulose hydrogel from NWB.

On the other hand, non-derivatising solvents (e.g. ionic liquids, organic solvents in the presence of inorganic salt and aqueous alkali solutions) dissolve cellulose by breaking down the inter- and intramolecular hydrogen bonds of cellulose (Medronho and Lindman, 2015). For example, ionic liquids can work by forming hydrogen bonds between the chloride anions in the solvent system and the hydrogen atoms of the cellulosic hydroxyl groups (Sayyed et al., 2019). The hydrogen bonds can also be disrupted by coordination interaction between the calcium ions in inorganic molten salt hydrates and the oxygen atoms of the cellulosic hydroxyl groups (Sen et al., 2013). In aqueous alkali solutions, the hydroxyl anions in this solvent can break the cellulose hydrogen bonding while the cations can stabilise the cellulose chains by binding to the cellulose hydroxyl group and inhibiting the reformation of hydrogen bonding (Xiong et al., 2013; Huang et al., 2019).

The aqueous alkali solvent (e.g. sodium hydroxide (NaOH) and lithium hydroxide aqueous alkali solution) has gained attention from the scientific community due to the ease of preparation, low-cost and less toxic nature (Kaco et al., 2014; Wong et al., 2021). Owing to these advantageous properties, this solvent has been widely used to prepare cellulose hydrogels from NWB including OPEFB, sugarcane bagasse, kenaf core and okara (Kaco et al., 2014; George et al., 2018; Salleh et al., 2018; Cui et al., 2019; Wong et al., 2021). Nonetheless, the cellulose depolymerisation mentioned above is usually required to improve cellulose dissolution

(Budtova and Navard, 2016; Wong et al., 2021). On top of that, adding urea or thiourea to the solvent can help to weaken the hydrophobic interaction of alkyl groups in cellulose, enhancing the cellulose dissolution (Zhou and Zhang, 2000; Zhang et al., 2002; Isobe et al., 2013; Xiong et al., 2014; Wernersson et al., 2015; Alves et al., 2016; Wang et al., 2017b; Alves et al., 2018).

1.5.3(d) Cellulose crosslinking

Both physical and chemical crosslinking methods have been demonstrated in previous studies to prepare cellulose hydrogels from NWB cellulose, namely cellulose from sugarcane bagasse, pineapple peel, OPEFB and kenaf core (Dai and Huang, 2017; Gan et al., 2017a; Salleh et al., 2018; Srirachya et al., 2018).

1.5.1(d)(i) Physical crosslinking

Although several physical crosslinking methods are mentioned in Section 1.4.2, only the phase inversion method has been employed to prepare NWB cellulose hydrogels in organic liquids with inorganic salt and ionic liquids (Dai et al., 2019; Srirachya et al., 2020). This process involves casting the cellulose solution on a supporting layer and precipitating cellulose by submerging it in a non-solvent bath. Eventually, the removal of solvent causes the cellulose polymers to transform from liquid to solid phase. No chemical crosslinker is required for crosslinking of cellulose in these processes. However, these physically crosslinked hydrogels exhibited a compact hydrogen-bonded cellulose network, limiting the water absorption ability of hydrogels (Wong et al., 2021).

1.5.1(d)(ii) Chemical crosslinking

Free radical polymerisation and etherification are the common chemical crosslinking methods that have been used to prepare NWB cellulose hydrogels. Generally, free radical polymerisation is a process in which monomers are polymerised with the aid of initiators (Ma et al., 2015). During initiation, initiators can generate active radical sites on cellulose chains, allowing the growth of polymer chains in the presence of crosslinkers. Free radical polymerisation can be initiated in various ways such as thermal degradation of persulphates, photolysis or ionising radiation (Wong et al., 2021). The reaction ceases when the monomers are depleted. Moreover, this method has the benefit of not requiring cellulose solubilisation and using water as the sole reaction medium (Ma et al., 2015).

Etherification with epichlorohydrin (ECH) has been employed to prepare OPEFB, kenaf core, okara and sugarcane bagasse cellulose hydrogels in alkali solvents (Kaco et al., 2014; George et al., 2018; Salleh et al., 2018; Cui et al., 2019; Wong et al., 2021). ECH is a chlorinated epoxy compound usually involved in the manufacture of synthetic glycerin used to synthesise pharmaceuticals, cosmetics and emulsifying agents (Weissermel and Arpe, 2003; Mota and Gimenez, 2022). ECH has a high chemical reactivity mainly due to the presence of three electrophilic carbon atoms and a high ring strain (Figure 1.9) (Singh et al., 2013).

Figure 1.9 Chemical structure of ECH (*electrophilic carbon atoms)

The crosslinking of cellulose by ECH happens via a condensation reaction which is also similar to the other types of crosslinkers such as aldehyde (e.g. glutaraldehyde) and polycarboxylic acid (e.g. citric acid) (Mota and Gimenez, 2022).

Nonetheless, cellulose-based materials prepared with ECH have advantageous properties over glutaraldehyde and citric acid in terms of hydrolytic stability and cost (Mota and Gimenez, 2022). On top of that, crosslinking with ECH has been reported in forming different cellulose-based materials including hydrogels, films, membranes and beads (Bai and Li, 2006; Guo et al., 2013; Shi et al., 2019; Mota and Gimenez, 2022).

During crosslinking, the etherification reaction between the hydroxyl groups of cellulosic chains is catalysed by the NaOH as depicted in Figure 1.10 (De Miguel et al., 1999). The ring of the epoxide of ECH is opened after the nucleophilic attack of the alkali cellulose on ECH (Figure 1.10B). Subsequently, the rearrangement of the structure gives rise to a new epoxide that can react with the new alkali cellulose to form cellulose ether (Figure 1.10C and Figure 1.10D).

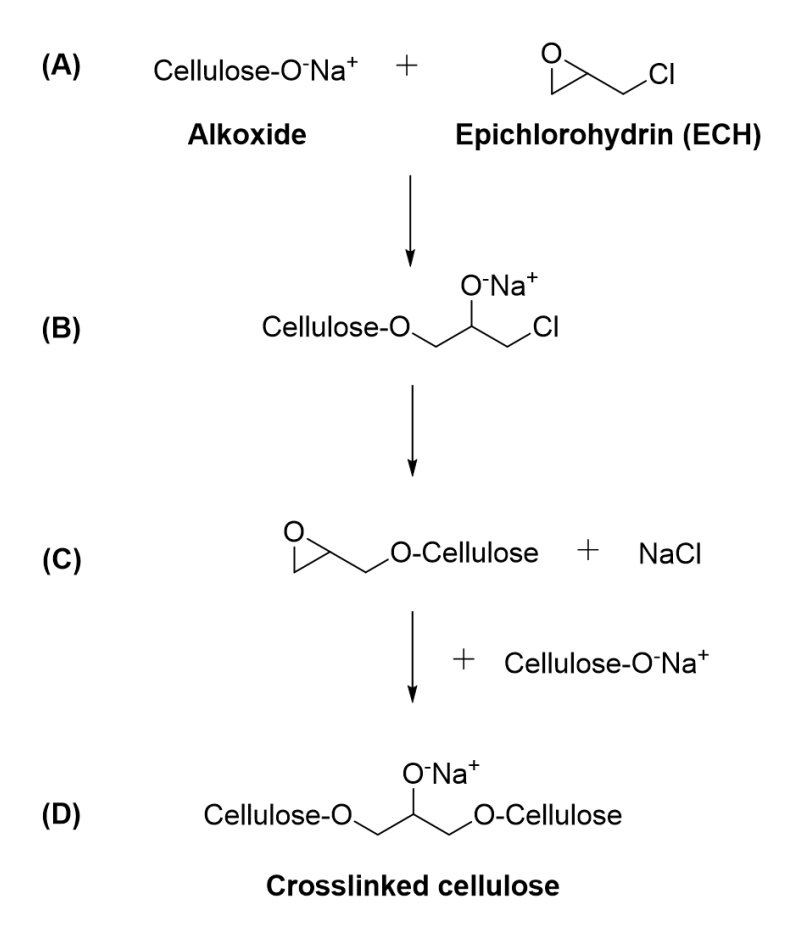


Figure 1.10 Proposed mechanism of crosslinking method of cellulose chains via etherification using ECH (adapted from De Miguel et al. (1999))

The highly reactive structure of ECH allows the formation of chemically stable ether bonds between the hydroxyl groups of cellulose chains. Yet, the highly reactive nature of ECH can also become toxic to humans especially when in contact with human skin (Sienel et al., 2000; Deutsche Forschungsgemeinschaft, 2003). Although ECH is cytotoxic, the safety of cellulose-based materials synthesised with ECH may not be a concern after the washing process with copious amounts of water to remove traces of unreacted ECH and byproducts (Yoshino et al., 1964; Wong et al., 2021; Mota and Gimenez, 2022; Wong et al., 2023).

1.6 Nanoemulsions (NEs)

Emulsions are colloidal systems consisting of two immiscible liquid phases, where a minor portion of one phase (dispersed phase) is distributed into a major portion of the other phase (continuous phase) (Patel et al., 2017). Emulsions are commonly stabilised using surfactants which reduce the interfacial tension between oil and water phases (Tadros et al., 2004; Singh et al., 2017; Witayaudom and Klinkesorn, 2017; Sarheed et al., 2020). The size of conventional emulsions usually ranges from 1 to 100 μm. In contrast, advanced emulsions such as NEs and microemulsions have smaller sizes ranging from several nanometres to a few hundred nanometres (Cheaburu-Yilmaz et al., 2019). While the formation of NEs requires a lower amount of surfactant (3 − 10%) than microemulsions (≥ 20%), NEs are less likely to have toxicity issues in food, pharmaceutical and cosmetics applications due to a low surfactant concentration used (Bouchemal et al., 2004; Thakore et al., 2012; Patel et al., 2017; Che Marzuki et al., 2019).

1.6.1 Types of NEs

NEs can be categorised into three types based on the compositions of oil and water: oil-in-water (o/w) NEs in which oil droplets are dispersed in a continuous

aqueous phase (Figure 1.11A), water-in-oil (w/o) NEs in which water droplets are disseminated in the continuous oil phase (Figure 1.11B) and bicontinuous NEs in which microdomains of oil and water are inter-dispersed within the system (Figure 1.11C) (Sutradhar and Amin, 2013; Singh et al., 2017).

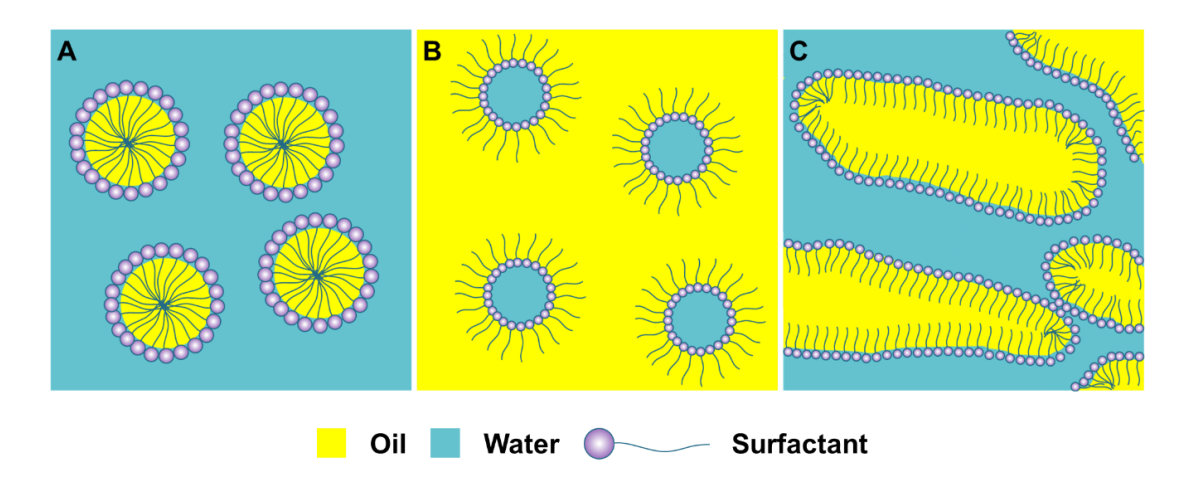


Figure 1.11 Structures of (A) oil-in-water, (B) water-in-oil and (C) bicontinuous NEs

Both o/w and w/o NEs have unique properties that make them suitable for specific applications. O/w NEs are extensively employed in various applications such as drug delivery, food and cosmetics due to their ability to enhance the solubility and bioavailability of poorly water-soluble actives (Liu et al., 2019). Moreover, they can be formulated in various forms including creams, liquids and sprays. They can also mask the unpleasant taste of ingredients in products (Azmi et al., 2019). Conversely, w/o NEs are less frequently used than o/w NEs and are typically used to protect encapsulated hydrophilic actives that are prone to degradation (Rabelo et al., 2018; Donsì and Velikov, 2019; Akram et al., 2021).